

Deposition of Functionalized Cr₇Ni Molecular Rings on Graphite from the Liquid Phase

By Alberto Ghirri,* Valdis Corradini, Christian Cervetti, Andrea Candini, Umberto del Pennino, Grigore Timco, Robin J. Pritchard, Christopher A. Muryn, Richard E. P. Winpenny, and Marco Affronte

Graphite is a clean substrate and its nanostructures hold great potential for applications. Anchoring large molecules on graphite represents a challenge for several reasons that essentially rise from the planar bonds of the packed honeycomb structure of carbon. Here, a systematic investigation by AFM and XPS on different derivatives of molecular Cr₇Ni rings deposited on highly oriented pyrolytic graphite (HOPG) is reported. Cr₇Ni is emerging as a prototypical example of molecular antiferromagnet on which quantum phenomena and coherence have been demonstrated. For the deposition of Cr₇Ni on HOPG, two strategies are adopted: 1) Cr₇Ni rings are functionalized with extended alkyl/benzene terminations and 2) a self-assembled monolayer of alkyl chains with sulfonate terminations is deposited and then a cationic Cr₇Ni derivative is used. In both cases the electronic bond with the carbon surface is soft, but the two-step procedure is efficient, albeit indirect, in sticking molecular Cr₇Ni on HOPG. These strategies can be easily extended to deposit other complex molecular aggregates on graphite from the liquid phase.

1. Introduction

Molecular nanomagnets can be tailored at the synthetic level and they allow a wide range of functionalizations of the external shell. This has led, for instance, to a rich collection of works devoted at defining differently functionalized derivatives of Mn₁₂, the prototypical single molecule magnet (SMM).^[1] Strategies to graft molecular nanoparticles^[2] or heterometallic antiferromagnetic molecular rings^[3] have also been developed. Altogether these

molecular nanomagnets represent an opportunity for possible applications as molecular devices for storing or processing information.^[4,5] Whether a single molecule may actually retain its main features while grafted on a surface is not a trivial issue and indeed experiments have shown that Mn₁₂ tends to be reduced on gold.^[6] Recent encouraging results have been obtained for sub-monolayers of Fe₄^[7] and Cr₇Ni^[8] that both seem to keep their main magnetic features even when deposited as isolated molecules on a surface.

A great deal of effort has been devoted so far to graft molecules on gold and semi-conducting (Si) surfaces.^[9] More recently nanostructured graphene sheets are attracting much interest due to their potentialities in electronics and nanotechnologies.^[10] Grafting molecules on single- or few-layer graphitic layers (nanotubes or graphene) requires, however, special care since any

covalent bond strongly modifies their structural and the electronic properties. In this case molecules need to be physisorbed on a carbon surface without forming chemical bonds. For highly oriented pyrolytic graphite (HOPG), the deposition of organic derivatives has been extensively investigated and reported in literature. Several organic molecules, ranging from alkane chains^[11] to phthalocyanines^[12] and other aromatic complexes,^[13] can order on self-assembled monolayers, exploiting either van der Waals or π - π interactions. In particular, drop-cast solutions of ferromagnetic bis(phthalocyaninato)terbium(III) molecules form ordered 2D arrays on HOPG.^[14] Adsorption of more complex (heavier) nanostructures is still possible from the liquid phase^[15–19] but weak bonds with the surface often result in a scarce immobilization of the clusters with consequent problems in the use of scanning probe microscopy.^[20]

Here we report on the synthesis and on the deposition on HOPG of different derivatives of heterometallic Cr₇Ni rings, molecular nanomagnets that show quantum phenomena^[21] and that have recently attracted much interest as suitable candidates for qubit encoding.^[4,5,22] We also explore an alternative route for the deposition of macromolecules from liquid phase involving the preparation of a buffer layer with higher affinity with the substrate. This procedure consists of two steps: 1) a self-assembled monolayer (SAM) of alkane sulfonates is deposited on HOPG

[*] Dr. A. Ghirri, Dr. V. Corradini, Dr. A. Candini
CNR-Institute of NanoSciences S3
via Campi 213/a, 41100 Modena (Italy)
E-mail: alberto.ghirri@unimore.it

C. Cervetti, Prof. U. del Pennino, Prof. M. Affronte
CNR-Institute of NanoSciences S3 and Dipartimento di Fisica
Università di Modena e Reggio Emilia
via Campi 213/a, 41100 Modena (Italy)

Dr. G. Timco, Dr. R. J. Pritchard, Dr. C. A. Muryn,
Prof. R. E. P. Winpenny
The Lewis Magnetism Laboratory
School of Chemistry, The University of Manchester
Oxford Road, Manchester M139PL (UK)

DOI: 10.1002/adfm.200902437

and 2) suitable cationic clusters are immobilized on the anionic SAM. While the interaction between the surface and the buffer layer remains of pure electrostatic type, ionic interactions between the buffer layer and the overlayer can help to stabilize the latter.

2. Results

Polycrystalline samples were synthesized as described in the experimental section. Namely they have chemical formulae $[(C_3H_7)_2NH_2][Cr_7NiF_8(O_2CR)_{16}]$, where $R = (C_2H_5)CH(CH_2)_3CH_3$ (1; $Cr_7Ni-eth$), $CH_3(CH_2)_8CH(CH_2)_6CH_3$ (2; $Cr_7Ni-hep$), $o-C_6H_5OC_6H_4$ (3; $Cr_7Ni-phe$), $(CH_3)_2CHC$ (4; $Cr_7Ni-dim$), and $[(C_3H_7)_2NH_2][Cr_7NiF_8\{O_2CCHC(CH_3)_2\}_{15}\{O_2CCH_2N(CH_3)_3\}]PF_6$ (5; $Cr_7Ni-bet$) (Fig. 1). Susceptibility versus temperature curves of different derivatives show a behavior close to the pristine compound $[(CH_3)_2NH_2][Cr_7NiF_8(O_2CC(CH_3)_3)_{16}](Cr_7Ni-piv)$ (see Supporting Information, Fig. 1S), thus indicating that the intensity of the intramolecular interactions is essentially preserved by the different functionalizations. Deposition on HOPG is inspected by means of atomic force microscopy (AFM) and X-ray photoemission spectroscopy (XPS), which give complementary information on topography and chemical composition of surfaces.

2.1. One-Step Deposition Protocol

2.1.1. AFM

For the deposition on HOPG, polycrystalline powders of $Cr_7Ni-eth$, $Cr_7Ni-hep$, and $Cr_7Ni-phe$ were dissolved in toluene at a given molar concentration, and then the substrate was dipped into the solution for 1 h. Figure 2A–I summarizes the AFM images obtained for the $Cr_7Ni-eth$, $Cr_7Ni-hep$, and $Cr_7Ni-phe$ derivatives deposited following this procedure. In order to limit the tip–surface interaction, images were taken at reduced tapping force. Horizontal panels show images taken on the same derivative and by varying the molar concentration of the solution. The surface coverage increases with the concentration regardless of the different spatial organization of the deposits. Molecules tend to self-assemble while isolated clusters cannot be discerned even at low concentrations. More specifically, Figure 2A, D, and G show that highly concentrated solutions (10^{-3} M) gives high coverage, as expected. For $Cr_7Ni-eth$ and $Cr_7Ni-phe$, Figure 2A and G show a compact overlayer, while for $Cr_7Ni-hep$ Figure 2D displays agglomerates and uncovered regions. By reducing the molarity down to 10^{-4} M, sub-monolayers become evident: Figure 2B and E shows that for $Cr_7Ni-eth$ and $Cr_7Ni-hep$ molecules self-assemble in flat 2D islands. These spots are often located close to edges or cleavage defects of the HOPG substrates. Conversely, Figure 2H shows for $Cr_7Ni-phe$ the deposition of small 3D aggregates distributed above the HOPG terraces, which display heights of a few nanometers and lateral size in the range between 10 and 100 nm. Line profiles (Fig. 2J) show that the height of the islands in Figure 2B and E is compatible with the size of the clusters,^[23] thus suggesting that these structures are formed by a single-layer of molecules. The different behavior observed for the deposits of $Cr_7Ni-phe$ could be explained by the presence of stronger intermolecular interactions, which may favor the formation of 3D aggregates. Reduction to 10^{-5} M molar

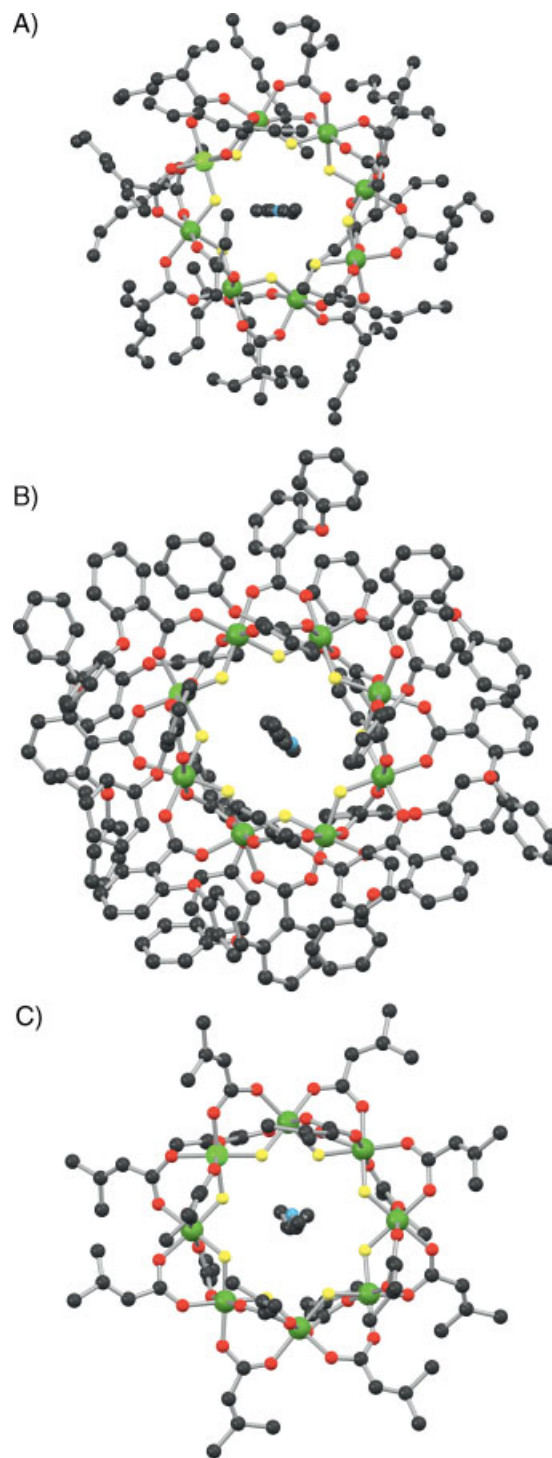


Figure 1. Crystallographic structures of different Cr_7Ni derivatives. A) $Cr_7Ni-eth$, B) $Cr_7Ni-phe$, and C) $Cr_7Ni-dim$. Cr and Ni: green; F: yellow; O: red; C: black; N: cyan. H-atoms are omitted for clarity.

concentration leads to a further decrease of the quantity of physisorbed material. For $Cr_7Ni-eth$ and $Cr_7Ni-hep$ Figure 2C and F show the presence of islands similar to those observed for 10^{-4} M, but with smaller sizes and lower incidence. For $Cr_7Ni-phe$, Figure 2I shows the HOPG surface nearly free of deposits.

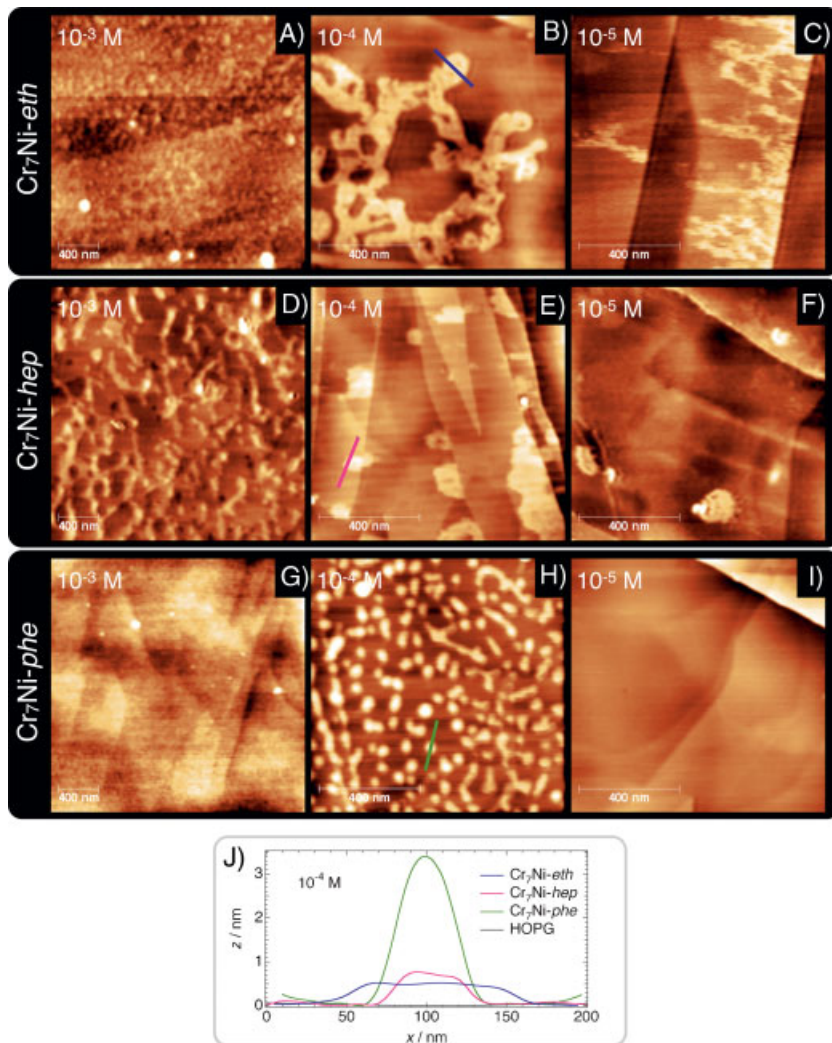


Figure 2. A–I) AFM images showing HOPG substrates decorated with functionalized $\text{Cr}_7\text{Ni-eth}$, $\text{Cr}_7\text{Ni-hep}$, and $\text{Cr}_7\text{Ni-phe}$ clusters. Samples are prepared by dipping the substrate in solutions with different molar concentrations. Scan area is $2.5 \times 2.5 \mu\text{m}^2$ for (A), (D), and (G) and $1 \times 1 \mu\text{m}^2$ for the others. J) Profiles measured along the lines drawn in panels (B), (E), and (H). The line profile measured on a clean HOPG terrace is plotted as a reference.

2.1.2. XPS

AFM results are confirmed by quantitative XPS investigations. Figure 3 shows the comparison among the core levels of the HOPG surface immersed for 1 h in a solution of $\text{Cr}_7\text{Ni-eth}$, $\text{Cr}_7\text{Ni-hep}$, and $\text{Cr}_7\text{Ni-phe}$. The intensities of the spectra are normalized taking into account the atomic sensitivity and the attenuation of the electronic signal. The Cr 2p, F 1s, Ni 2p, and O 1s core level line-shapes measured for the different systems fit well to the corresponding spectra obtained for a multilayer deposited from the liquid phase (not shown here). For each system the ratios of F/Cr, Cr/Ni, and Cr/O are well reproducible and close to the expected values (Table 1), indicating that the ring stoichiometry is preserved in the different runs. The observed small excess of oxygen is likely due to adventitious oxygen.

From the C 1s/Cr 2p ratio (Table 1) we derived the average area occupied by each cluster, subtracting the different number of C

atoms for each molecule and taking into account the signal attenuation due to the presence of the overlayer. These values were obtained by assuming that the molecules lay flat on the surface and considering for the $\text{Cr}_7\text{Ni-eth}$, $\text{Cr}_7\text{Ni-hep}$, and $\text{Cr}_7\text{Ni-phe}$ clusters an area of 3.5, 5.3, and 4.5 nm^2 , respectively. The corresponding values of coverage are in agreement with those extracted from the AFM studies (Table 1).

The O 1s core level region of $\text{Cr}_7\text{Ni-phe}$ is characterized by a broad, asymmetric peak with a marked shoulder on the high binding energy (BE) side (Fig. 3). The O 1s fitting procedure was performed using two Voigt functions with the same broadening (Lorentzian and Gaussian widths of 0.55 and 1.5 eV). The predominant component at 532.6 eV (O_1) is assigned to the oxygen in the carboxylate group (COOH),^[24] while the low-intensity component at 533.7 eV (O_2) is assigned to the oxygen that bonds the two benzene rings (C–O–C). The fact that the intensity of O_1 is twice of O_2 fits well with the stoichiometry of the molecule (32 oxygen in the carboxylate and 16 in the C–O–C site). Conversely the O 1s of $\text{Cr}_7\text{Ni-eth}$ and $\text{Cr}_7\text{Ni-hep}$ are characterized by a single peak at about 532.6 eV, in agreement with the fact that only the oxygen of the carboxylate are present in these molecules.

XPS experiments show that the overlayers deposited with the one-step procedure can be removed by long (minutes) rinse in solvent. This indicates that the molecule–HOPG interaction is weak as expected for this type of molecular functionalization.

2.2. Two-Step Deposition Protocol

In order to obtain a stronger sticking of Cr_7Ni rings on the HOPG surface, we have developed a two-step procedure (Fig. 4A and B), the key idea of which is to deposit charged Cr_7Ni rings onto a HOPG surface previously functionalized with an anionic SAM. In practice, we first treat the surface of HOPG with $\text{CH}_3(\text{CH}_2)_{15}\text{SO}_3\text{Na}$ (C_{16}SO_3), an anionic surfactant molecule that shows both a hydrophobic alkyl chain that easily adsorbs on HOPG and a hydrophilic SO_3^- functional group that easily coordinates with a water molecule. Highly packed $\text{C}_{16}\text{SO}_3^-$ SAMs (coverage close to 100%) are prepared on HOPG by soaking the substrate in a diluted solution (2×10^{-5} M) of C_{16}SO_3 in water for 10 min.^[25,26] In the second step, immobilization of the cationic magnetic molecules onto this anionic $\text{C}_{16}\text{SO}_3^-$ SAM was obtained by dipping the so-prepared substrate in a diluted solution (10^{-4} M) of $\text{Cr}_7\text{Ni-bet}$. Starting from $\text{Cr}_7\text{Ni-dim}$, $\text{Cr}_7\text{Ni-bet}$ was obtained by replacing one dimethylacrylate end-group with a betaine, where a cationic NH_3^+ functional group is neutralized by PF_6^- (see experimental section).

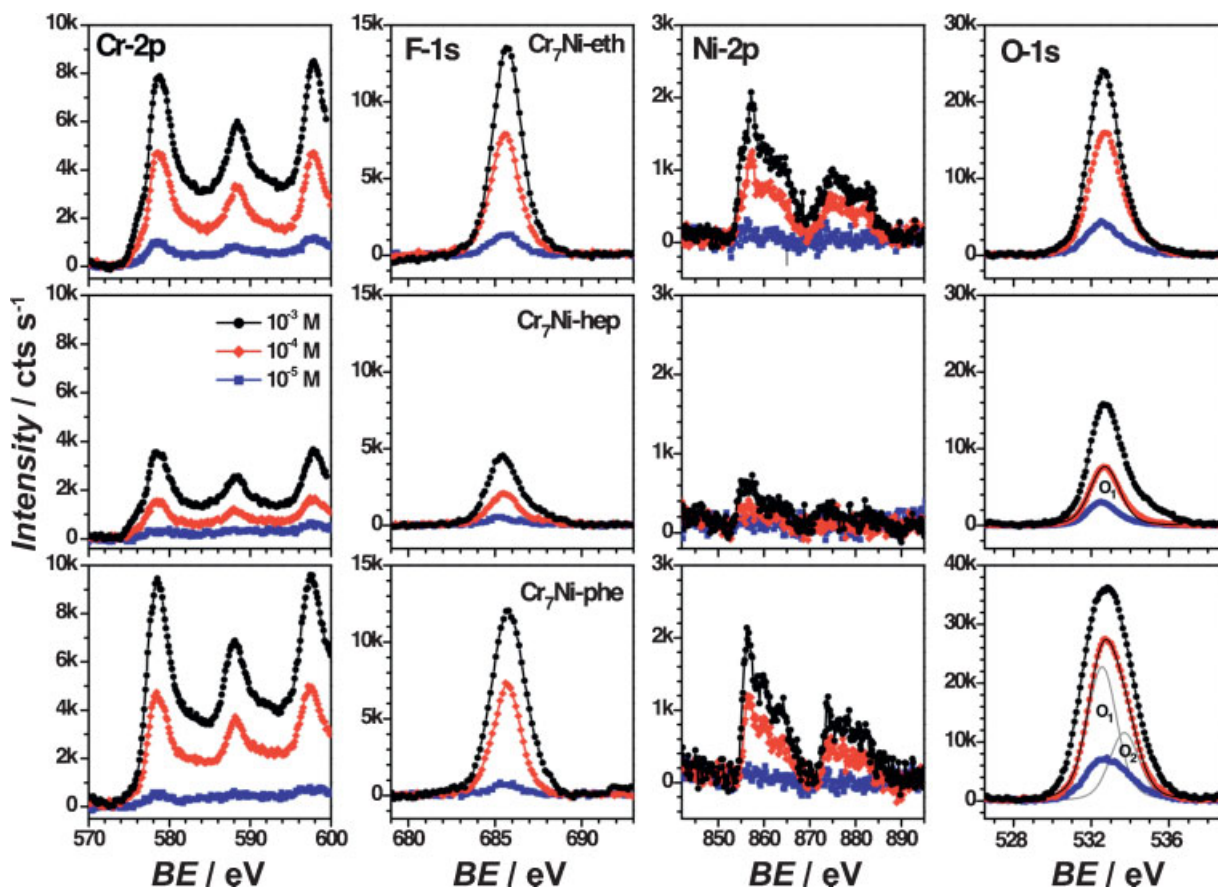


Figure 3. Core level XPS spectra obtained for the HOPG substrates immersed in solutions of $\text{Cr}_7\text{Ni-eth}$ (upper panels), $\text{Cr}_7\text{Ni-hep}$ (central panels), and $\text{Cr}_7\text{Ni-phe}$ (lower panels) with different concentrations (10^{-3} , 10^{-4} , and 10^{-5} M).

2.2.1. AFM

We used AFM for checking the protocol at different steps of the deposition (Fig. 4C–F). A surface of freshly cleaved HOPG graphite is shown in Figure 4C. After dipping the HOPG substrate in the solution of C_{16}SO_3 (Fig. 4D), the AFM image shows the presence of an adsorbed monolayer with roughness of about 0.3 nm (Fig. 4G) due to the self-assembling of C_{16}SO_3 molecules lying flat on the surface, in agreement with the literature.^[25] The

sample is then immersed for 1 min in $\text{Cr}_7\text{Ni-bet}$ solution (Fig. 4E). The deposits form structures with height ranging between 2 and 3 nm (Fig. 4G). Further rinsing with solvent removes the exceeding clusters. The optimal result with the lower number of 3D aggregates is obtained upon rinsing in pure dichloromethane for 10 min and drying under N_2 flux (Fig. 4F). The image shows the surface decorated with structures having height of about 1 nm. Considering the enlargement due to the AFM tip, line profiles in

Table 1. Stoichiometric values derived from the core level intensities of the $\text{Cr}_7\text{Ni-eth}$, $\text{Cr}_7\text{Ni-hep}$, and $\text{Cr}_7\text{Ni-phe}$ for three different concentrations (10^{-3} , 10^{-4} , and 10^{-5} M). The expected stoichiometric values are reported in brackets. The average area occupied by each Cr_7Ni ring on the HOPG surface and the comparison between the coverage of Cr_7Ni derived from XPS and estimated from the AFM images are also shown.

Derivative	Molarity [M]	F 1s/Cr 2p [7.0]	Cr 2p/Ni 2p [1.14]	O 1s/7Cr 2p	C 1s/Cr 2p ($\times 10^3$)	Area/molecule [nm^2]	Coverage Cr_7Ni [%]	
							XPS	AFM
$\text{Cr}_7\text{Ni-eth}$	10^{-3}	6.8 ± 0.5	1.15 ± 0.05	28 [32]	5	6	60 ± 10	65 ± 10
	10^{-4}	7.1 ± 0.5	1.12 ± 0.05	30 [32]	11	11	35 ± 5	22 ± 10
	10^{-5}	6.9 ± 0.5	1.16 ± 0.05	48 [32]	70	50	8 ± 5	13 ± 5
$\text{Cr}_7\text{Ni-hep}$	10^{-3}	6.9 ± 0.5	1.15 ± 0.05	40 [32]	12	12	50 ± 10	43 ± 10
	10^{-4}	6.8 ± 0.5	1.13 ± 0.05	43 [32]	20	19	30 ± 5	15 ± 5
	10^{-5}	7.3 ± 0.5	1.10 ± 0.05	50 [32]	80	60	10 ± 5	5 ± 5
$\text{Cr}_7\text{Ni-phe}$	10^{-3}	6.8 ± 0.5	1.13 ± 0.05	54 [48]	3	5	90 ± 10	–
	10^{-4}	6.7 ± 0.5	1.12 ± 0.05	58 [48]	9	10	50 ± 10	35 ± 10
	10^{-5}	6.6 ± 0.5	1.10 ± 0.05	53 [48]	96	66	7 ± 5	0 ± 5

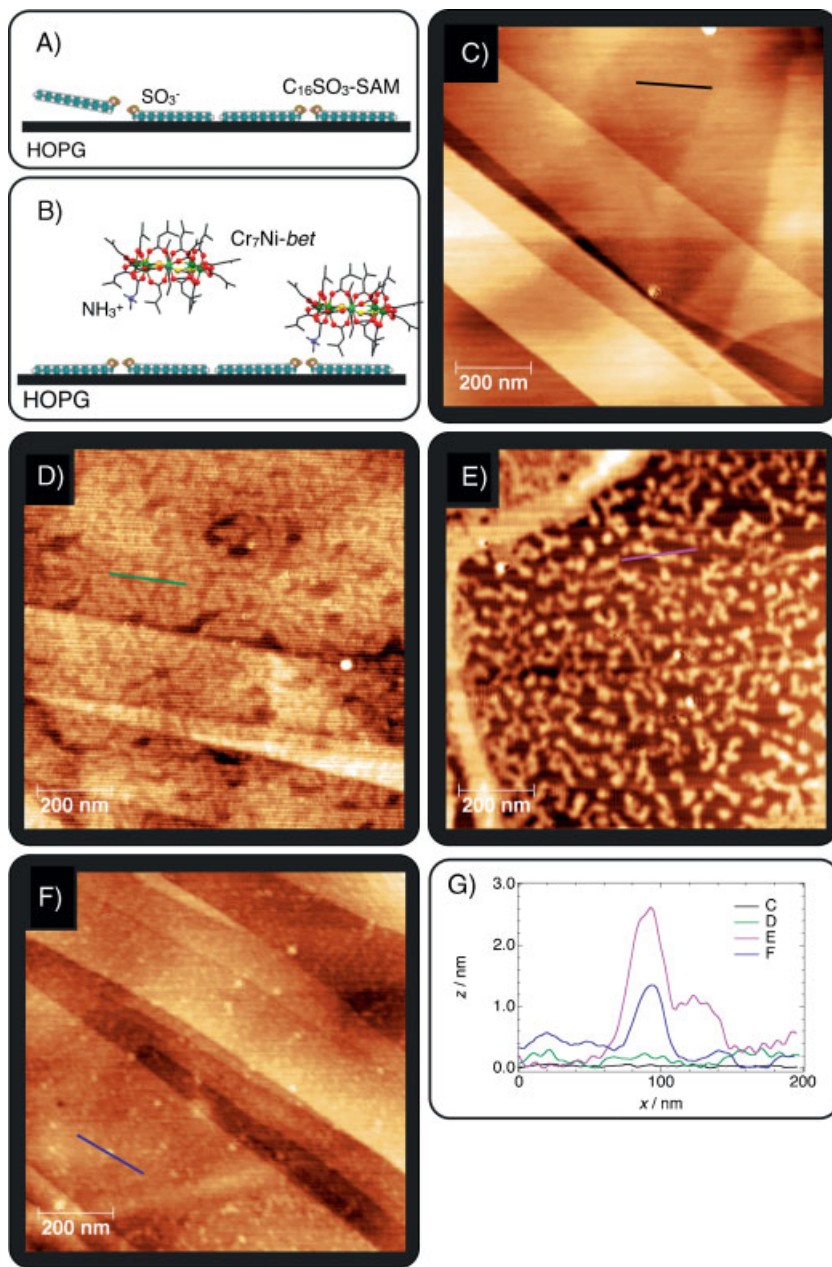


Figure 4. Schematic of the two-step procedure for the deposition of functionalized molecules of $\text{Cr}_7\text{Ni-bet}$. A) First step. B) Second step. AFM images taken at subsequent stages of the two-step deposition protocol described in the text. C) Clean HOPG surface. D) Image taken after dipping in solution of $\text{C}_{16}\text{SO}_3/\text{water}$ (first step). E) Image taken after dipping in solution of $\text{Cr}_7\text{Ni-bet}/\text{acetonitrile}$ (second step). F) Image taken after rinsing for 10 min in dichloromethane. G) Comparison among the line profiles taken along the solid lines drawn in panels (C–F).

Figure 4G are actually consistent with the size of isolated $\text{Cr}_7\text{Ni-bet}$ clusters.

2.2.2. XPS

We used XPS for a quantitative study of the two-step protocol. In Figure 5 we compare the S 2p, Cr 2p, and F 1s core levels measured after the first step (C_{16}SO_3), the second step ($\text{Cr}_7\text{Ni-bet}$), and the

rinse in dichloromethane (for 10 s, 1 min, and 10 min). The core level line-shapes fit well the corresponding spectra obtained for a multilayer deposited from the liquid phase, and the F/Cr, Cr/Ni, and Cr/O ratios are reproducible and close to the expected values, demonstrating that ring stoichiometry is preserved. The presence of the S 2p_{3/2} component at about 168.5 eV reveals the presence of a sulfur atom involved in the sulfonate groups.^[27]

From the C 1s/S 2p and C 1s/Cr 2p ratios (Table 2), subtracting the different numbers of C atoms for each molecule and taking into account the signal attenuation due to the presence of the overlayer, we derived both the packing of the $\text{C}_{16}\text{SO}_3\text{-SAM}$ and the average area occupied by each Cr_7Ni cluster. These values were obtained assuming that the molecules lay flat on the surface, where an area (height) of 1.0 nm^2 (0.5 nm) and 3.1 nm^2 (1.3 nm) has been considered respectively for C_{16}SO_3 ^[25,26] and $\text{Cr}_7\text{Ni-bet}$. In Table 2 the corresponding values of coverage for both $\text{C}_{16}\text{SO}_3\text{-SAM}$ and $\text{Cr}_7\text{Ni-bet}$ are reported. For the latter the coverage results are in good agreement with the values estimated from the AFM images. The variations of the S 2p/C 1s and Cr 2p/C 1s ratios with respect to the duration of the rinse (Fig. 5D) reveal i) the presence of a stable $\text{C}_{16}\text{SO}_3\text{-SAM}$ with a coverage that remains rather constant between 60% and 70% and ii) the presence of a Cr_7Ni overlayer with a coverage that remains above the 15% even after a heavy rinse. These findings can be explained with the presence of an effective bond between $\text{C}_{16}\text{SO}_3\text{-SAM}$ and molecules of $\text{Cr}_7\text{Ni-bet}$.

2.2.3. Further AFM and XPS Experiments

Further cross checks of this crucial point were performed with supplementary AFM and XPS experiments. Initially we modified the first step, and thus the $\text{Cr}_7\text{Ni-bet}$ derivative was either directly deposited on HOPG without $\text{C}_{16}\text{SO}_3\text{-SAM}$ or deposited on neutral buffer layers made of simple alkane chains or amines. In particular we employed tetratriacontane $\text{C}_{34}\text{H}_{70}$ (C_{34}) and octadecylamine $\text{CH}_3(\text{CH}_2)_{17}\text{NH}_2$ (C_{18}NH_2) (see experimental section). In these cases, AFM images show that the deposited $\text{Cr}_7\text{Ni-bet}$ is promptly removed by

rinsing with dichloromethane solvent, thus suggesting that the clusters are weakly immobilized when the buffer layer of C_{16}SO_3 is not employed. XPS experiments confirm this outcome and in Figure 6 the Cr 2p core levels are compared before and after the 10 min rinse in dichloromethane. Contrary to what happens when the clusters of $\text{Cr}_7\text{Ni-bet}$ are deposited on the $\text{C}_{16}\text{SO}_3\text{-SAM}$ (Fig. 6A), for $\text{Cr}_7\text{Ni-bet}$ deposited directly on HOPG (Fig. 6D) and

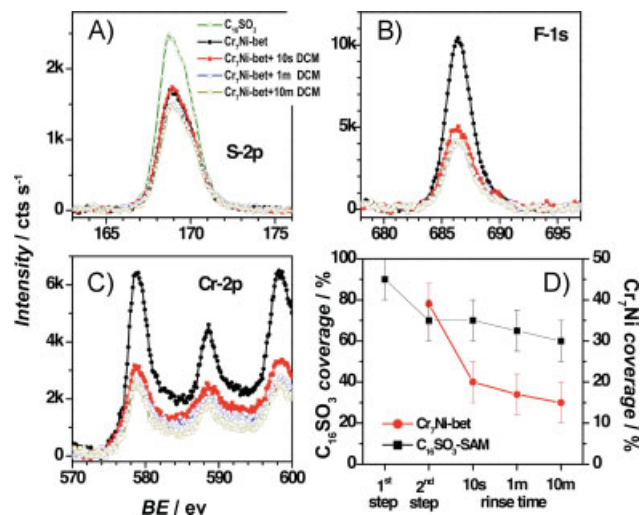


Figure 5. A–C) Core level XPS spectra of the HOPG surface after the first step of $C_{16}SO_3$ /water (open triangles), the second step of Cr_7Ni -bet/dichloromethane (filled circles), and after the rinse in dichloromethane for 10 s (filled squares), 1 min (open circles), and 10 min (open squares). D) Values of coverage derived from the C 1s/S 2p and C 1s/Cr 2p ratios taken for both $C_{16}SO_3$ -SAM and the Cr_7Ni -bet overlayer and shown after the first step, the second step, and the rinse of respectively 10 s, 1 min, and 10 min.

on neutral buffer layers of C_{34} (Fig. 6C) and $C_{18}NH_2$ (Fig. 6B), the spectra show the vanishing of the Cr 2p core level after the rinse.

In a further set of experiments we modified the second step and non-functionalized Cr_7Ni -piv, Cr_7Ni -met, and Cr_7Ni -dim clusters were deposited in place of Cr_7Ni -bet on the $C_{16}SO_3$ -SAM. Cr_7Ni -dim is the precursor of Cr_7Ni -bet before the substitution of the betaine termination (see experimental section) and Cr_7Ni -met ($[(C_3H_7)_2NH_2][Cr_7NiF_8(O_2C_4H_5)_{16}]$) is obtained as reported in the

literature.^[28] Figure 6 shows that the pristine Cr_7Ni -piv is completely removed by the 10 min immersion in dichloromethane, which does not occur in the case of Cr_7Ni -dim and Cr_7Ni -met, where the rinse leaves about 10% of the surface covered with clusters (Fig. 6F, Table 2). AFM images confirm the outcome of the XPS experiments. The effect of the substitution of one dimethylacrylate end-group with the betaine can be directly evaluated by the comparison between the AFM images of the deposited overlayers of Cr_7Ni -dim and Cr_7Ni -bet (see Supporting Information, Fig. 4S). In detail, while for Cr_7Ni -bet the surface is covered with a uniform 2D overlayer, for Cr_7Ni -dim the clusters tend to aggregate in 3D islands and to leave uncovered regions. These results confirm that the anionic SO_3^- terminations of $C_{16}SO_3$ -SAM selectively interact with the cationic betaine of Cr_7Ni -bet and, albeit less effectively, with the unsaturated carboxylate ligands in Cr_7Ni -met, Cr_7Ni -dim, and Cr_7Ni -bet, but not with pristine, electrically neutral, Cr_7Ni -piv.

4. Conclusions

The deposition on HOPG from the liquid phase of different heterometallic Cr_7Ni molecular rings with formulae $[(C_3H_7)_2NH_2][Cr_7NiF_8(O_2CR)_{16}]$ were studied in detail by the complementary surface techniques AFM and XPS. Surface coverage is comparable to that obtained with other substrates (e.g., gold) but the sticking of these derivatives is rather weak as can be deduced by the fact that they are removed after a long rinse. We thus implement a more efficient protocol that uses a preliminary deposition of a SAM of molecules with sulfonate functional groups that are able to capture cationic derivatives and, less efficiently, peripheral unsaturated ligands of selected Cr_7Ni derivatives. We present several experiments to cross check these points and support this conclusion. These results demonstrate that liquid-

Table 2. Summary of the system investigated within the two-step approach. a) Reference values of the first step deposited from solution of $C_{16}SO_3$ /water. b) Second step deposited from solution of Cr_7Ni -bet/dichloromethane on $C_{16}SO_3$ -SAM. c) Cr_7Ni -bet deposited directly on HOPG and on buffer layers of $C_{18}NH_2$ (d) and C_{34} (e). Deposition of Cr_7Ni -piv/dichloromethane (f), Cr_7Ni -dim/dichloromethane (g), and Cr_7Ni -met/dichloromethane (h) on $C_{16}SO_3$ -SAM. The coverage of the $C_{16}SO_3$ -SAM and Cr_7Ni ring derived from the C 1s/S 2p and C 1s/Cr 2p ratios, in good agreement with the values estimated from the AFM images, are also reported.

Code	Step 1	Step 2	Rinse	C 1s/S 2p	Coverage $C_{16}SO_3$ [%]	C 1s/7Cr 2p	Coverage Cr_7Ni [%]	
							XPS	AFM
a	$C_{16}SO_3$	–	no	150	95 ± 5	–	–	–
b	$C_{16}SO_3$	Cr_7Ni -bet	no	220	70 ± 5	1600	38 ± 5	41 ± 10
	$C_{16}SO_3$	Cr_7Ni -bet	10 s	230	70 ± 5	3300	20 ± 5	–
	$C_{16}SO_3$	Cr_7Ni -bet	1 min	240	65 ± 5	3500	17 ± 5	20 ± 10
	$C_{16}SO_3$	Cr_7Ni -bet	10 min	250	60 ± 5	3900	15 ± 5	7 ± 5
	–	Cr_7Ni -bet	no	–	–	1200	45 ± 10	42 ± 10
c	–	Cr_7Ni -bet	10 min	–	–	31000	1 ± 5	0 ± 5
	$C_{18}NH_2$	Cr_7Ni -bet	no	–	–	2500	23 ± 5	–
d	$C_{18}NH_2$	Cr_7Ni -bet	10 min	–	–	16000	3 ± 5	0 ± 5
	C_{34}	Cr_7Ni -bet	no	–	–	4800	11 ± 5	–
e	C_{34}	Cr_7Ni -bet	10 min	–	–	20000	2 ± 5	0 ± 5
	$C_{16}SO_3$	Cr_7Ni -piv	no	190	80 ± 5	4100	15 ± 5	–
f	$C_{16}SO_3$	Cr_7Ni -piv	10 min	200	75 ± 5	23000	2 ± 5	–
	$C_{16}SO_3$	Cr_7Ni -dim	no	230	70 ± 5	1700	35 ± 5	25 ± 10
g	$C_{16}SO_3$	Cr_7Ni -dim	10 min	240	65 ± 5	5000	11 ± 5	5 ± 5
	$C_{16}SO_3$	Cr_7Ni -met	no	240	65 ± 5	2100	29 ± 5	–
h	$C_{16}SO_3$	Cr_7Ni -met	10 min	230	70 ± 5	6700	9 ± 5	–

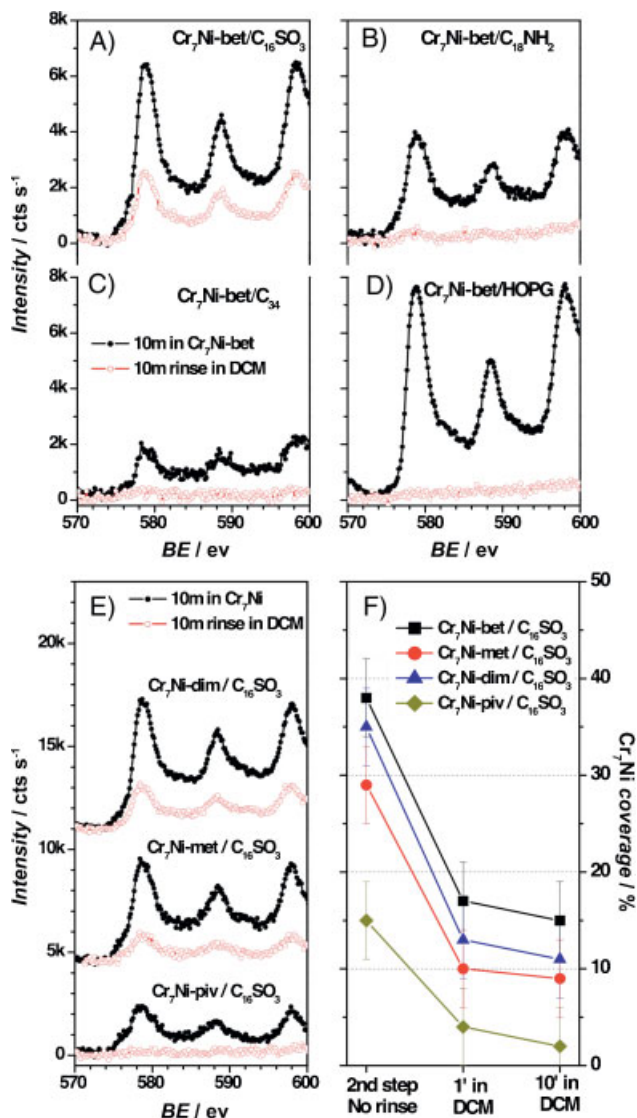


Figure 6. Cr 2p core levels, before (filled circles) and after (open circles) the rinse in dichloromethane (10 min) for clusters of Cr₇Ni-*bet* deposited on C₁₆SO₃-SAM (A), on neutral buffer layers C₁₈NH₂ (B) and C₃₄ (C), and directly on the HOPG surface (D). E) Cr 2p core levels before (filled circles) and after (open circles) the rinse in dichloromethane (10 min) for clusters Cr₇Ni-*dim*, Cr₇Ni-*met*, and Cr₇Ni-*piv* deposited on C₁₆SO₃-SAM. F) Dependence of the coverage of Cr₇Ni-*bet* deposited on C₁₆SO₃-SAM with respect to the duration of the rinse.

phase deposition can be used and optimized to deposit large molecules on graphite. Since carbon-based nanostructured materials have great potentialities for future applications, our results may contribute to opening alternative ways for assembling hybrid multifunctional materials.

5. Experimental

Compound Synthesis: Unless stated otherwise, all reagents and solvents were purchased from commercial sources and used without further purification. The syntheses of 1–4 were carried out in Erlenmeyer Teflon

FEP flasks supplied by Fisher. Column chromatography was carried out using Silicagel LC60A (particle size 40–63 μm) from Fluorochem as the stationary phase using a positive pressure of air, and thin-layer chromatography (TLC) was performed on precoated silica gel plates (0.25-mm-thick, 60 F₂₅₄, Merck, Germany). Betaine hexafluorophosphate salt (betHPF₆) was prepared as previously reported [29].

Compounds 1–4 were prepared by a variation of the procedure published in Reference [30] by carrying out the reaction of CrF₃ · 4H₂O in a mixture of (C₃H₇)₂NH, 2NiCO₃ · 3Ni(OH)₂ · 4H₂O and a large excess of respective carboxylic acid (2-ethylhexanoic acid, 2-heptylundecanoic acid, 2-phenoxybenzoic acid, or 3,3-dimethylacrylic acid). In all these compounds the transition metal ions are bridged by fluoride and two 1,3-bridging carboxylates. The Ni site is disordered over all possible metal sites. Crystallographic structures are drawn respectively in Figure 1. Cr₇Ni-*eth* is a flat disk with diameter of about 2.1 nm and height of about 1.0 nm. Aromatic groups can be employed as well, and with 2-phenoxybenzoic acid this gives rise to compound Cr₇Ni-*phe* (Fig. 1B), which has a diameter of about 2.4 nm and height of about 1.4 nm. Starting from Cr₇Ni-*dim* (Fig. 1C), we replace one dimethylacrylate ligand with a betaine ligand, thus obtaining Cr₇Ni-*bet*, where the cationic betaine functional group is neutralized by the PF₆⁻. Crystallographic data (excluding structure factors) for the structures reported in this paper have been deposited with the Cambridge Crystallographic Data Centre as supplementary publication no. CCDC 759426-759428.

Compound (1): CrF₃ · 4H₂O (5.0 g, 27.62 mmol), 2-ethylhexanoic acid (10 g, 69.34 mmol), di-*n*-propylamine (1.4 g, 13.84 mmol), and 2NiCO₃ · 3Ni(OH)₂ · 4H₂O (0.6 g, 1.02 mmol) were heated together under stirring at 160 °C for 7 h. During this period a green viscous mass was formed. Then the flask was cooled and toluene (15 mL) was added and stirred for 1 h at 100 °C. The toluene was removed by distillation and the temperature was increased to 160 °C to heat the flask for a further 24 h. After this, the flask was cooled to room temperature (R.T.) and product extracted in dichloromethane (75 mL). The extract was filtered and the solvent removed under reduced pressure, and then acetonitrile (200 mL) was added to the obtained residue while stirring for 24 h at R.T. The product was collected by filtration and washed copiously with acetonitrile and dried *en vacuo*, then extracted in hexane. Further purification of 1 was performed by column chromatography using hexane/toluene 1.5:1 as the eluent and it was eluted as the first main band. The solvents were then evaporated under reduced pressure. Yield: 6.54 g (56%, based on Cr). Suitable crystals for X-ray structure characterization were obtained by slow evaporation of a diluted solution of 1 in acetone. Anal. calcd for C₁₃₄H₂₅₆Cr₇F₈N₁Ni₁O₃₂: Cr 12.26, Ni 1.98, C 54.22, H 8.69, N 0.47; found: Cr 12.45, Ni 1.89, C 54.05, H 9.07, N 0.42.

Compound (2): Cr₇Ni-*hep* was prepared by an analogous procedure to that for 1 by using 2-heptylundecanoic acid instead of 2-ethylhexanoic acid and in purification of 2 by column chromatography first hexane was used as solvent to elute an unidentified brown-greenish band. Thereafter hexane/toluene elution was used. Pure 2 was obtained as the second band starting its elution with 1:10 and finishing with 1:5 hexane/toluene. 2 is sticky (viscid) and all attempts to get crystals were unsuccessful. Yield: 5.4 g (26%, based on Cr). Anal. calcd for C₂₉₄H₅₇₆Cr₇F₈N₁Ni₁O₃₂: Cr 6.98, Ni 1.13, C 67.75, H 11.14, N 0.27; found: Cr 6.85, Ni 1.02, C 68.20, H 10.68, N 0.24.

Compound (3): CrF₃ · 4H₂O (2.0 g, 11.05 mmol), 2-phenoxybenzoic acid (10 g, 46.68 mmol), dipropylamine (0.7 g, 6.92 mmol), and 2NiCO₃ · 3Ni(OH)₂ · 4H₂O (0.2 g, 0.34 mmol) were heated at 140 °C for 6 h with stirring. During this period a green solid was formed. After this the flask was cooled to R.T. and acetonitrile added (30 mL) with stirring. The obtained precipitate was collected by filtration and washed with a large quantity of acetonitrile and dried *en vacuo*. The product was recrystallized from toluene/acetonitrile. Yield: 3.2 g (50% based on Cr). Anal. calcd for C₂₁₄H₁₆₀Cr₇F₈N₁Ni₁O₄₈: Cr 8.90, Ni 1.44, C 62.87, H 3.94, N 0.34; found: Cr 8.61, Ni 1.27, C 62.98, H 3.97, N 0.30.

Compound (4): Cr₇Ni-*dim* was prepared by an analogous procedure to that for 3 by using 3,3-dimethylacrylic acid instead of 2-phenoxybenzoic acid; the reaction time was 10 h, and then the product was extracted in diethyl ether (100 mL). The extract was filtered and the solvent removed

under reduced pressure, and the obtained residue dissolved in hot acetonitrile (50 mL), solution filtered, and the filtrate diluted slowly while stirring with H₂O (50 mL) at R.T. The crystalline product started to form immediately. The flask was kept at R.T. for one day, then the crystals were collected by filtration, washed copiously with H₂O and a mixture of MeCN/H₂O (1:1) and dried *en vacuo*. Yield: 2.5 g (70% based on Cr). Anal. calcd for C₈₆H₁₂₈Cr₇F₈N₁Ni₁O₃₂: Cr 16.09, Ni 2.59, C 45.65, H 5.70, N 0.62; found: Cr 15.73, Ni 2.32, C 45.70, H 5.65, N 0.54. ES MS (sample dissolved in MeCN, run in MeOH): +2262 [M]⁺; +2285 [M + Na]⁺ (100%).

Compound (5): 4 (2.0 g 0.88 mmol), betHPF₆ (1.0 g 3.8 mmol), and acetonitrile (50 mL) were refluxed for 74 h with constant stirring. The resulting solution was cooled to R.T. and filtered. The solvent from the filtrate was removed under reduced pressure and the residue was stirred with toluene (~300 mL) for 24 h, then filtered and the solid washed with diethyl ether. Then it was dissolved in acetone (~50 mL). The acetone extract was filtered and evaporated to dryness giving a green solid that was washed with H₂O and then dried *en vacuo*. The product was recrystallized from MeCN/toluene to give a microcrystalline solid, which was washed with diethyl ether and then dried *en vacuo*. Yield: 0.72 g (34% based on 4). Anal. calcd for C₈₆H₁₃₂Cr₇F₁₄N₂Ni₁O₃₂P₁: Cr 15.01, Ni 2.42, C 42.59, H 5.49, N 1.15; found: Cr 14.54, Ni 2.05, C 42.60, H 5.19, N 1.38. ES MS (sample dissolved in MeCN, run in MeOH): +2280 [M-PF₆]⁺ (100%).

Deposition: We used HOPG substrates purchased from NT-MDT (grade ZYA) that were freshly cleaved before use.

One-Step Procedure: Microcrystalline powders of Cr₇Ni-*eth*, Cr₇Ni-*hep*, or Cr₇Ni-*phe* were dissolved in toluene with different concentrations. The HOPG substrate was dipped for 1 h into the solution and then dried under N₂ gas. Preparatory tests showed that dipping times as long as two days do not increase the coverage of the surface, while short times (1 min) reduce the quantity of deposited material but do not allow the decoration of the surface with dispersed molecules. A long (minutes) rinse in toluene may result in efficient washing away of clusters from the HOPG surface.

Two-Step Procedure: SAMs of C₁₆SO₃ were obtained by dipping the HOPG substrate in a solution of water (2 × 10⁻⁵ M) for 10 min and drying under N₂ flux. XPS spectra show that Na 1s/S 2p core level ratio is only 0.1 instead of 1, suggesting that polar water molecules can associate with sulfonate groups and replace Na⁺ [25]. Alternative deposition of C₁₆SO₃ from a solution of acetonitrile shows a stoichiometric Na/S ratio (but lower coverage of HOPG). In the second step, microcrystalline powders of Cr₇Ni-*bet* were dissolved either in dichloromethane or acetonitrile with concentration 10⁻⁴ M. We studied two alternative deposition protocols: a) dipping in C₁₆SO₃/water for 10 min, N₂ flux, dipping in Cr₇Ni-*bet*/dichloromethane for 1 min, N₂ flux and b) dipping in C₁₆SO₃/water for 10 min, N₂ flux, dipping in Cr₇Ni-*bet*/acetonitrile for 1 min, N₂ flux. Both protocols give comparable AFM and XPS results, with the minor exception that acetonitrile dissolves a small amount of the C₁₆SO₃-SAM, resulting in a slightly lower coverage. The effect on the value of coverage of HOPG for an increased immersion time of 10 min in Cr₇Ni-*bet*/dichloromethane is negligible with respect to 1 min. Deposition of C₃₄ was performed from toluene solution (10⁻⁴ M). Deposition of C₁₈NH₂ was performed from ethanol solution (10⁻⁴ M). C₁₈SO₃ was purchased from Fluka. C₃₄ and C₁₈NH₂ were purchased from Sigma. Solvents are HPLC grade and water is Ultrapure Millipore purified.

Characterization: AFM images were collected in air by means of a NanoScope III (Veeco) working in tapping mode. We used golden Si probes (NT-MDT) having resonant frequency of about 150 kHz and nominal radius of curvature of 10 nm. XPS measurements were performed using an Omicron hemispherical analyzer (EA125) and a Mg K α X-ray source ($h\nu = 1253.6$ eV). Susceptibility measurements were carried out on powders by means of a Quantum Design Physical Properties Measurement System with an AC excitation field of 10 Oe and frequency of 90, 1730, and 9300 Hz.

Acknowledgements

This work was carried out within the framework of the EU Network of Excellence MAGMANet contract No. 515767 and supported by the FP7-ICT

FET Open "MolSpinQIP" project, contract No. 211284, and by the EPSRC (UK). We thank R. Biagi, V. de Renzi, and P. Torelli for assistance during the experiments. Supporting Information is available online from Wiley InterScience or from the authors.

Received: December 24, 2009

Revised: February 12, 2010

Published online: April 14, 2010

- a) D. Ruiz-Molina, M. Mas-Torrent, J. Gómez, A. I. Balana, N. Domingo, J. Tejada, M. T. Martínez, C. Rovira, J. Veciana, *Adv. Mater.* **2003**, *15*, 42.
- b) E. Coronado, A. Forment-Aliaga, F. M. Romero, V. Corradini, R. Biagi, V. de Renzi, A. Gambardella, U. del Pennino, *Inorg. Chem.* **2005**, *44*, 7693.
- c) R. V. Martínez, F. García, R. García, E. Coronado, A. Forment-Aliaga, F. M. Romero, S. Tatay, *Adv. Mater.* **2007**, *19*, 291.
- d) Z. Salman, K. H. Chow, R. I. Miller, A. Morello, T. J. Parolin, M. D. Hossain, T. A. Keeler, C. P. D. Levy, W. A. MacFarlane, G. D. Morris, H. Saadaoui, D. Wand, R. Sessoli, G. G. Condorelli, R. F. Kiefl, *Nano Lett.* **2007**, *7*, 1551.
- B. Fleury, F. Volatron, L. Catala, D. Brinzei, E. Rivière, V. Huc, C. David, F. Miserque, G. Rogez, L. Baraton, S. Palacin, T. Mallah, *Inorg. Chem.* **2008**, *47*, 1898.
- V. Corradini, R. Biagi, U. del Pennino, V. de Renzi, A. Gambardella, M. Affronte, C. Muryn, G. Timco, R. E. P. Winpenny, *Inorg. Chem.* **2007**, *46*, 4968.
- F. Troiani, A. Ghirri, M. Affronte, S. Carretta, P. Santini, G. Amoretti, S. Piligkos, G. Timco, R. E. P. Winpenny, *Phys. Rev. Lett.* **2005**, *94*, 207208.
- G. A. Timco, S. Carretta, F. Troiani, F. Tuna, R. J. Pritchard, C. A. Muryn, E. J. L. McInnes, A. Ghirri, A. Candini, P. Santini, G. Amoretti, M. Affronte, R. E. P. Winpenny, *Nat. Nanotechnol.* **2009**, *4*, 173.
- M. Mannini, P. Sainctavit, R. Sessoli, C. Cartier dit Moulin, F. Pineider, M.-A. Arrio, A. Cornia, D. Gatteschi, *Chem. -Eur. J.* **2008**, *14*, 7387.
- M. Mannini, F. Pineider, P. Sainctavit, C. Danieli, E. Otero, C. Sciancalepore, A. M. Talarico, M.-A. Arrio, A. Cornia, D. Gatteschi, R. Sessoli, *Nat. Mater.* **2009**, *8*, 194.
- V. Corradini, F. Moro, R. Biagi, V. De Renzi, U. del Pennino, V. Bellini, S. Carretta, P. Santini, V. A. Milway, G. Timco, R. E. P. Winpenny, M. Affronte, *Phys. Rev. B* **2009**, *79*, 144419.
- B. Fleury, L. Catala, V. Huc, C. David, W. Z. Zhong, P. Jegou, L. Baraton, S. Palacin, P.-A. Albouy, T. Mallah, *Chem. Commun.* **2005**, 2020.
- a) L. Bogani, W. Wernsdorfer, *Nat. Mater.* **2008**, *7*, 179. b) L. Bogani, C. Danieli, E. Biavardi, N. Bendiab, A.-L. Barra, E. Dalcanales, W. Wernsdorfer, A. Cornia, *Angew. Chem. Int. Ed.* **2008**, *48*, 746.
- a) J. P. Rabe, S. Buchholz, *Science* **1991**, *253*, 424. b) C. L. Claypool, F. Faglioni, W. A. Goddard, III, H. B. Gray, N. S. Lewis, R. A. Marcus, *J. Phys. Chem. B* **1997**, *101*, 5978.
- a) X. Qiu, C. Wang, Q. Zeng, B. Xu, S. Yin, H. Wang, S. Xu, C. Bai, *J. Am. Chem. Soc.* **2000**, *122*, 5550. b) B. Xu, S. Yin, C. Wang, X. Qiu, Q. Zeng, C. Bai, *J. Phys. Chem. B* **2000**, *104*, 10502. c) X.-H. Kong, K. Deng, Y.-L. Yang, Q.-D. Zeng, C. Wang, *J. Phys. Chem. C* **2007**, *111*, 17382.
- S. De Feyter, C. De Schryver, *J. Phys. Chem. B.* **2005**, *109*, 4290.
- J. Gomez-Segura, I. Diez-Perez, N. Ishikawa, M. Nakano, J. Veciana, D. Ruiz-Molina, *Chem. Commun.* **2006**, 2866.
- S. Deng, J. Locklin, D. Patton, A. Baba, R. C. Advincula, *J. Am. Chem. Soc.* **2005**, *127*, 1744.
- M. Rolandi, K. Scott, E. G. Wilson, F. C. Meldrum, *J. Appl. Phys.* **2001**, *89*, 1588.
- G. Bottari, D. Olea, C. Gómez-Navarro, F. Zamora, J. Gómez-Herrero, T. Torres, *Angew. Chem. Int. Ed.* **2008**, *47*, 2026.
- R. W. Saalfrank, A. Scheurer, I. Bernt, F. W. Heinemann, A. V. Postnikov, V. Schünemann, A. X. Trautwein, M. S. Alam, H. Rupp, P. Müller, *Dalton Trans.* **2006**, 2865.
- N. Hoshino, A. M. Ako, A. K. Powell, H. Oshio, *Inorg. Chem.* **2009**, *48*, 3396.
- L. Sun, R. M. Crooks, *Langmuir* **2002**, *18*, 8231.
- S. Carretta, P. Santini, G. Amoretti, M. Affronte, A. Ghirri, I. Sheikin, S. Piligkos, G. Timco, R. E. P. Winpenny, *Phys. Rev. B* **2005**, *72*, 060403(R).

- [22] A. Candini, G. Lorusso, F. Troiani, A. Ghirri, S. Carretta, P. Santini, G. Amoretti, C. Muryn, F. Tuna, G. Timco, E. J. L. McInnes, R. E. P. Winpenny, W. Wernsdorfer, M. Affronte, *Phys. Rev. Lett.* **2010**, *104*, 037203.
- [23] It is well known that height measurements performed with tapping mode AFM face several problems in terms of capillary forces and compression. For instance, for organic surfaces is generally gives apparent heights lower than the real ones (see, e.g., B. Basnar, G. Friedbacher, H. Brunner, T. Vallant, U. Mayer, H. Haffmann, *Appl. Surf. Sci.* **2001**, *171*, 213).
- [24] G. Gonella, S. Terreni, D. Cvetko, A. Cossaro, L. Mattera, O. Cavalleri, R. Rolandi, A. Morgante, L. Floreano, M. Canepa, *J. Phys. Chem. B* **2005**, *109*, 18003.
- [25] X.-L. Yin, L.-J. Wan, Z.-Y. Yang, J.-Y. Yu, *Appl. Surf. Sci.* **2005**, *240*, 13.
- [26] A. J. Kudelski, *Raman Spectrosc.* **2003**, *34*, 853.
- [27] C.-C. Han, W.-D. Hseih, J.-Y. Yeh, S.-P. Hong, *Chem. Mater.* **1999**, *11*, 480.
- [28] V. Di Noto, A. B. Boeer, S. Lavina, C. A. Muryn, M. Bauer, G. A. Timco, E. Negro, M. Rancan, R. E. P. Winpenny, S. Gross, *Adv. Funct. Mater.* **2009**, *19*, 3226.
- [29] E. Coronado, A. Forment-Aliaga, A. Gaita-Ariño, C. Giménez-Saiz, F. M. Romero, W. Wernsdorfer, *Angew. Chem. Int. Ed.* **2004**, *43*, 6152.
- [30] F. K. Larsen, E. J. L. McInnes, H. El Mkami, J. Overgaard, S. Piligkos, G. Rajaraman, E. Rentschler, A. A. Smith, G. M. Smith, V. Boote, M. Jennings, G. A. Timco, R. E. P. Winpenny, *Angew. Chem. Int. Ed.* **2003**, *42*, 101.